Vol. 472: 27–44, 2013
doi: 10.3354/meps10061

MARINE ECOLOGY PROGRESS SERIES
Mar Ecol Prog Ser

Published January 9

Filamentation and eddy–eddy interactions in marine larval accumulation and transport

Cheryl S. Harrison[1,*], David A. Siegel[2], Satoshi Mitarai[3]

[1]Earth and Planetary Sciences Department, University of California, Santa Cruz, California 95064, USA
[2]Earth Research Institute and Department of Geography, University of California, Santa Barbara, California 93106, USA
[3]Marine Biophysics Unit, Okinawa Institute of Science and Technology, Okinawa 904-0495, Japan

ABSTRACT: A coupled particle-tracking/ocean circulation model of an idealized eastern boundary upwelling current is used to explore the mesoscale pathways of larval transport. We find that simulated larvae are often organized into filaments found between mesoscale eddies that correspond to attracting Lagrangian coherent structures (LCS). Such structures are material curves that map filamentation and transport boundaries, often corresponding to the locations of sea-surface temperature fronts. Filamentation and eddy–eddy interactions aggregate larvae from many source regions and release times into small, highly dense packets that can be transported back to the shelf. Larval densities in these packets can be up to 2 orders of magnitude greater than initial release densities near the coast and are robust to strong levels of random 'swimming' perturbations. This study suggests that coherent flow structures play an important role in pelagic transport of marine larvae.

KEY WORDS: Larval transport · Lagrangian coherent structures · Coastal oceanography · Marine ecology · Fisheries

INTRODUCTION

Eastern boundary currents (EBCs) such as the California Current System (CCS) contain many of the most productive fisheries in the world (e.g. Ryther 1969, Chassot et al. 2010), and coastal waters in EBCs are important habitats and spawning grounds for many species of fishes and invertebrates (Parrish et al. 1981, Love et al. 2002). The elevated rate of productivity in EBCs is due to coastal upwelling, where equatorward coastal winds drive ocean surface transport offshore, bringing nutrient-rich water to the surface, thus driving primary productivity. Coastal upwelling also generates mesoscale coherent structures, notably upwelling filaments, jets and eddies (Flament et al. 1985, Brink & Cowles 1991, Haynes et al. 1993). These structures organize the transport of upwelled waters containing biologically important material such as nutrients, plankton and marine propagules (e.g. larvae, eggs, spores; Parrish et al. 1981, Larson et al. 1994, Rodriguez et al. 1999).

Ocean transport of propagules connects populations of many coastal marine species (Levin 2006, Cowen & Sponaugle 2009). Consequently, understanding marine propagule transport is important for a wide range of scientific and management problems, from assessment of recruitment dynamics and population genetics to fisheries management and marine conservation planning (e.g. Warner & Cowen 2002, Palumbi 2003, Botsford et al. 2009, Costello et al. 2010, Rassweiler et al. 2012). Marine propagules themselves are typically small (a few millimeters to a few centimeters) and require days to months in the plankton to develop competency for their next life stage (Strathmann 1985, Metaxas & Saunders 2009). While larvae of many species are capable of a variety of behaviors that can alter their dispersal patterns (Shanks 1985, Sponaugle et al. 2002), they are also

*Email: chsharrison@gmail.com

strongly affected by prevailing currents, where they are dispersed over spatial scales from 100s of meters to 100s of kilometers (e.g. Jackson & Strathmann 1981, Kinlan & Gaines 2003, Siegel et al. 2003, Shanks 2009). Current variability in EBCs is typically much stronger than the mean flow (Marchesiello et al. 2003, Harrison & Glatzmaier 2012) and depends on topographic, remote and seasonal forcing (Haynes et al. 1993, Hill et al. 1998, Marchesiello et al. 2003, Marchesiello & Estrade 2009), making the effect of eddies on dispersal both important and highly variable in space and time (Largier 2003, Mitarai et al. 2008, Siegel et al. 2008).

Larval transport has been commonly modeled as a diffusive process (e.g. Okubo 1980, Jackson & Strathmann 1981, Largier 2003), sometimes with the addition of mean flow advection (Roberts 1997, Gaylord & Gaines 2000, Siegel et al. 2003, Shanks 2009). This led to the idea of a Gaussian dispersion kernel to quantify larval transport (e.g. Largier 2003, Siegel et al. 2003), a concept that has been used extensively to inform ecosystem management practices (see Botsford et al. 2009 for a review). However, observations of larval settlement across many oceanographic regimes show that large, local, intermittent settlement events are common and that single events can dominate local recruitment for a year or more (Ebert & Russell 1988, Warner et al. 2000). This suggests the Gaussian kernel approach does not satisfactorily represent larval transport processes on time and space scales relevant to coastal marine populations (Mitarai et al. 2008, Siegel et al. 2008), and that resolving recruitment events driven by ocean variability is crucial to advancing understanding of dispersal and connectivity (Warner et al. 2000, Largier 2003, Botsford et al. 2009, Mitarai et al. 2009).

Recent approaches have utilized ocean circulation model flow fields, remote sensing observations, as well as a growing number of *in situ* observations to characterize larval transport and recruitment patterns more realistically than ever before (e.g. Bjorkstedt et al. 2002, Cowen et al. 2006, Aiken et al. 2007, Broitman et al. 2008, Mitarai et al. 2009, Watson et al. 2010, Aiken et al. 2011, Drake et al. 2011, Kim & Barth 2011, Woodson et al. 2012). These observations and models illustrate the large role that coherent flow structures (such as filaments and eddies) play in the transport of plankton, larvae and other propagules. In particular, several recent studies have highlighted the delivery of discrete 'packets' of larvae back to the nearshore as an important settlement process (e.g. Mitarai et al. 2008, Siegel et al. 2008), consistent with observations of episodic recruitment (Warner et al. 2000). The temporally intermittent and spatially heterogeneous patterns of larval settlement and connectivity seen in these studies are thought to have important consequences for metapopulation dynamics, species coexistence and optimal fisheries management (e.g. Berkley et al. 2010, Costello et al. 2010, Aiken & Navarete 2011, Bode et al. 2011, Watson et al. 2011a,b, 2012, Rassweiler et al. 2012). It has been hypothesized that the complex eddying dynamics of the coastal ocean are driving packet formation and subsequent transport (Siegel et al. 2008); however, the physical details remain largely unexplained.

The goal of this study is to explore the processes that control the generation and movement of filaments and larval packets. One of the hallmarks of ocean turbulence is eddy–eddy interaction and merger (McWilliams 1984, Bracco et al. 2004), moving energy from small to large scales and resulting in eddies from several 10s up to 200 km in diameter that can persist for weeks to years (Marchesiello et al. 2003, Chelton et al. 2007, Marchesiello & Estrade 2009, Harrison & Glatzmaier 2012). During eddy merger events, smaller eddies are entrained and filamented along the edges of larger eddies (McWilliams 1984, Harrison & Glatzmaier 2012). Here we find eddy interaction results in creation of dense, often long filamental packets of larvae that can bring together larvae of many ages and source regions into small, yet dense packets.

Our modeling system was created to replicate mesoscale dynamics off the Central California coast (Mitarai et al. 2008, Siegel et al. 2008) and, as such, captures many of the features common to all eastern boundary upwelling currents, such as the upwelling jet, its associated eddies and filaments, and a dynamic offshore eddy field (Hill et al. 1998, Marchesiello & Estrade 2009). The modeling framework consists of a 3-dimensional ocean circulation model, a particle-tracking model to keep track of simulated larvae, and an analytical tool from dynamical systems theory: Lagrangian coherent structures (LCS). LCS are used as a metric to map the attractors of the filamentation process, to visualize transport boundaries and eddy interactions, and to provide a framework for understanding the kinematics of ocean transport (d'Ovidio et al. 2004, Wiggins 2005, Samelson & Wiggins 2006, Beron-Vera et al. 2008, Shadden 2012). Our hypothesis is that attracting LCS (ALCS) will mark the dominant transport pathways of marine propagules. That is, larvae will be preferentially concentrated in 'larval superhighways' mapped by ALCS, as opposed to being 'diffusively', more uni-

formly, distributed, or within eddy interiors where there are few LCS. To the best of our knowledge, the utility of LCS have yet to be explored in the context of marine propagule transport, although LCS have been the focus of many recent studies of pollutant and biological transport in marine systems (e.g. Lehahn et al. 2007, 2011, Olascoaga et al. 2008, Rossi et al. 2009, Shadden et al. 2009, Tew Kai et al. 2009, Calil & Richards 2010, d'Ovidio et al. 2010, Katija et al. 2011, Huhn et al. 2012).

LAGRANGIAN COHERENT STRUCTURES (LCS)

Our goal in this section is to provide a brief conceptual introduction to LCS and to make a few specific points relevant to the methods and results presented here. We refer the interested reader to the introductory text by Abraham & Shaw (1992), reviews by Wiggins (2005), Shadden (2012), and Samelson (2013), the textbook by Samelson & Wiggins (2006), and an online tutorial (Shadden 2005) for more detailed information and examples.

LCS can be thought of as material lines moving with the ocean surface that act as transport barriers and map regions of active filamentation, effectively allowing us to visualize the skeleton of turbulent transport (e.g. Haller 2002, d'Ovidio et al. 2004, Shadden et al. 2005, Mathur et al. 2007, Beron-Vera et al. 2008, Shadden 2012). Broadly, particles on a surface will move toward and along an attracting LCS (ALCS) and away from and along a repelling LCS (RLCS). LCS are also ideally particle trajectories, so a particle will remain on an LCS once it encounters it (Video S1 in the supplement at www.int-res.com/articles/suppl/m472p027_supp/).

Trajectories of water parcels near LCS associated with a saddle (or stagnation) point are illustrated in Fig. 1a. Arrows indicate the instantaneous direction of movement of water parcel trajectories within the fluid. The blue lines represent ALCS, trajectories separating fluid parcels (on either side), that at this moment are close to each other, but in the recent past were much farther apart. That is, there is *confluence* of fluid particle trajectories near the ALCS (which is not necessarily a horizontal convergence or downwelling). The red lines in Fig. 1a represent RLCS, trajectories separating fluid parcels that will soon separate, that is, experience *diffluence* (and not necessarily divergence or upwelling). Near Lagrangian saddle points—the intersection of RLCS and ALCS—fluid parcels stretch out in time along the ALCS into a long, thin filament (Fig. 1a; gray features, see also Video S1 in the supplement). In this way the gradient of a passive tracer field can be intensified by the filamentation process without any horizontal convergence or associated downwelling. For buoyant particles (as used here) or, similarly, any planktonic material that maintains its position in the water column, any convergence will intensify the process of filamentation and lead to stronger gradients in tracer fields (e.g. Genin et al. 2005, Bakun 2010).

How are LCS calculated? Fluid parcels nearby, but not on, a LCS (Fig. 1a; black ovals, also see Video S1 in the supplement) move along and asymptotically toward the ALCS and away from the RLCS on hyper-

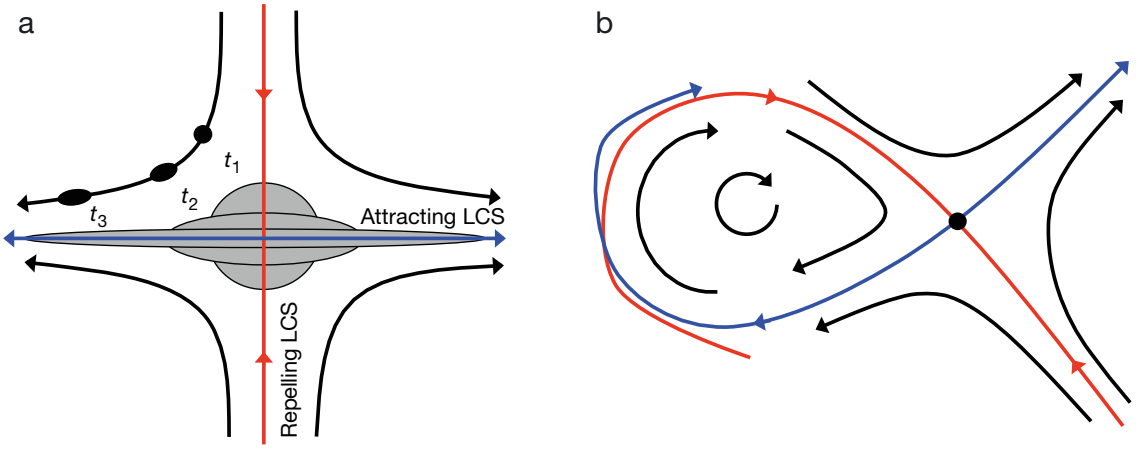

Fig. 1. Schematics of fluid/particle behavior near Lagrangian coherent structures (LCS). (a) Attracting (blue) and repelling (red) LCS often intersect at saddle points. Fluid initially surrounding the saddle point at time t_1 (gray circle) stretches out along the attracting LCS, forming a long, thin filament by t_3. Nearby fluid parcels (black) move along hyperbolic trajectories (solid black lines), remaining relatively unstretched through time. (b) Attracting and repelling LCS surrounding an eddy are commonly nearly coincident, often forming a complex tangle of intersections (see also Fig. 2a and Video S1 in the supplement available at www.int-res.com/articles/suppl/m472p027_supp/)

bolic trajectories (black lines). Along these trajectories neighboring fluid parcels are strained differing amounts by the flow field. These differences in stretching rates allow the detection of LCS by the Lyapunov exponent, which quantifies the rate that neighboring particles separate. Here we use the finite-time Lyapunov exponent (FTLE) (Haller 2002, Shadden et al. 2005), although other methods have been developed (d'Ovidio et al. 2004, Mancho et al. 2006). In essence, the FTLE is a scalar field that measures the time-averaged local exponential rate of particle separation. The FTLE is calculated by seeding the fluid velocity field with a dense, uniform grid of passive tracer particles, integrating their trajectories, and tracking the separation of particles initially nearby through time (the relative dispersion). Particles on either side of an LCS will move apart at an exponential rate as they move away from the saddle point, i.e.:

$$\Delta\mathbf{x}(t = t_0 + T) = \Delta\mathbf{x}(t = t_0)\exp(\lambda T)$$

where $\Delta\mathbf{x}(t)$ is the distance between 2 particles at time t, $T = t - t_0$ is the particle trajectory integration time, and $\Delta\mathbf{x}(t = t_0)$ is the initial separation. The local finite-time Lyapunov exponent is found by solving for the exponent λ:

$$\lambda = 1/|T| \ln||\Delta\mathbf{x}(t_0 + T)/\Delta\mathbf{x}(t_0)||$$

where λ is a scalar function of the particle release location, the time (t_0), and the integration time (T). The magnitude of the deformation gradient $||\Delta\mathbf{x}(t_0 + T)/\Delta\mathbf{x}(t_0)||$ is found by identifying the square root of the maximal singular value (i.e. the maximum stretching factor) at each initial particle location (Haller 2002, Shadden et al. 2005). LCS are identified from FTLE scalar fields as high values or ridges. RLCS are found by evolving particle trajectories forward in time ($T > 0$), while ALCS are found by evolving particle trajectories backward in time ($T < 0$). Longer integration times effectively grow the LCS away from the saddle points, heightening and thinning the LCS (e.g. Fig. 5 in Harrison & Glatzmaier 2012). Here we use an initial particle separation of 500 m and an integration time of 14 d, more than long enough to grow the LCS so that the relevant flow features are visualized.

The implication of LCS being material curves is that fluid moving along an LCS will stay on this curve and not pass across it (Video S1 in the supplement). Thus, ideally LCS act as transport barriers for passive particles and tracers advected by large-scale flow (Shadden et al. 2005). LCS can map long-lived fronts separating ocean water masses with different characteristics (e.g. temperature, salinity, oxygen). While temperature or density fronts imply a transport barrier is present, the converse is not necessarily true, and LCS may map transport barriers that are not associated with fronts. However, for ocean flows in near-geostrophic balance, LCS and fronts will likely coincide.

RLCS are often found nearly coincident with ALCS, especially around eddies (Figs. 1b & 2a). This coincidence should be expected. For time-invariant systems, ALCS associated with one saddle point often form the RLCS of another saddle point (heteroclinic trajectories), or even circle back and attach to the same saddle point (homoclinic trajectories). Thus, an LCS can be both attracting and repelling at the same time, with respect to different source materials (Abraham & Shaw 1992, Samelson & Wiggins 2006). However, this connectivity breaks up with perturbation (Abraham & Shaw 1992, Wiggins 2005, Samelson & Wiggins 2006). In general, we expect ALCS and RLCS on the ocean surface should, in many cases, be close to each other, but not coincide exactly (Figs. 1b & 2a). This will become important in the statistical analysis to follow.

MODELS

The CCS-in-a-box model, implemented in the Regional Ocean Modeling System (ROMS) (Shchepetkin & McWilliams 2005), was designed to replicate the mesoscale eddy dynamics of central California coastal circulation in a simplified domain (Mitarai et al. 2008, Siegel et al. 2008). The 3-dimensional model domain features a north/south periodic (wrap-around) boundary, an open western boundary, and a narrow shelf (~10 km) along a straight eastern boundary coastline. A constant alongshore pressure gradient is imposed within the model which creates a poleward undercurrent. The model is forced by variable wind stress that replicates the temporal wind variability off Central California during summer upwelling (a typical July). A total of 28 runs with different wind stress time series (with identical wind stress statistics) were created to represent interannual variability in upwelling forcing. Implementation details for the CCS-in-a-box model can be found in Mitarai et al. (2008) and Siegel et al. (2008).

Marine propagules are modeled as quasi-Lagrangian tracer ocean particles originating from the shelf region. They are constrained to remain on the top ocean model layer, a common strategy for many marine propagules (e.g. Love et al. 2002). This simplifies the

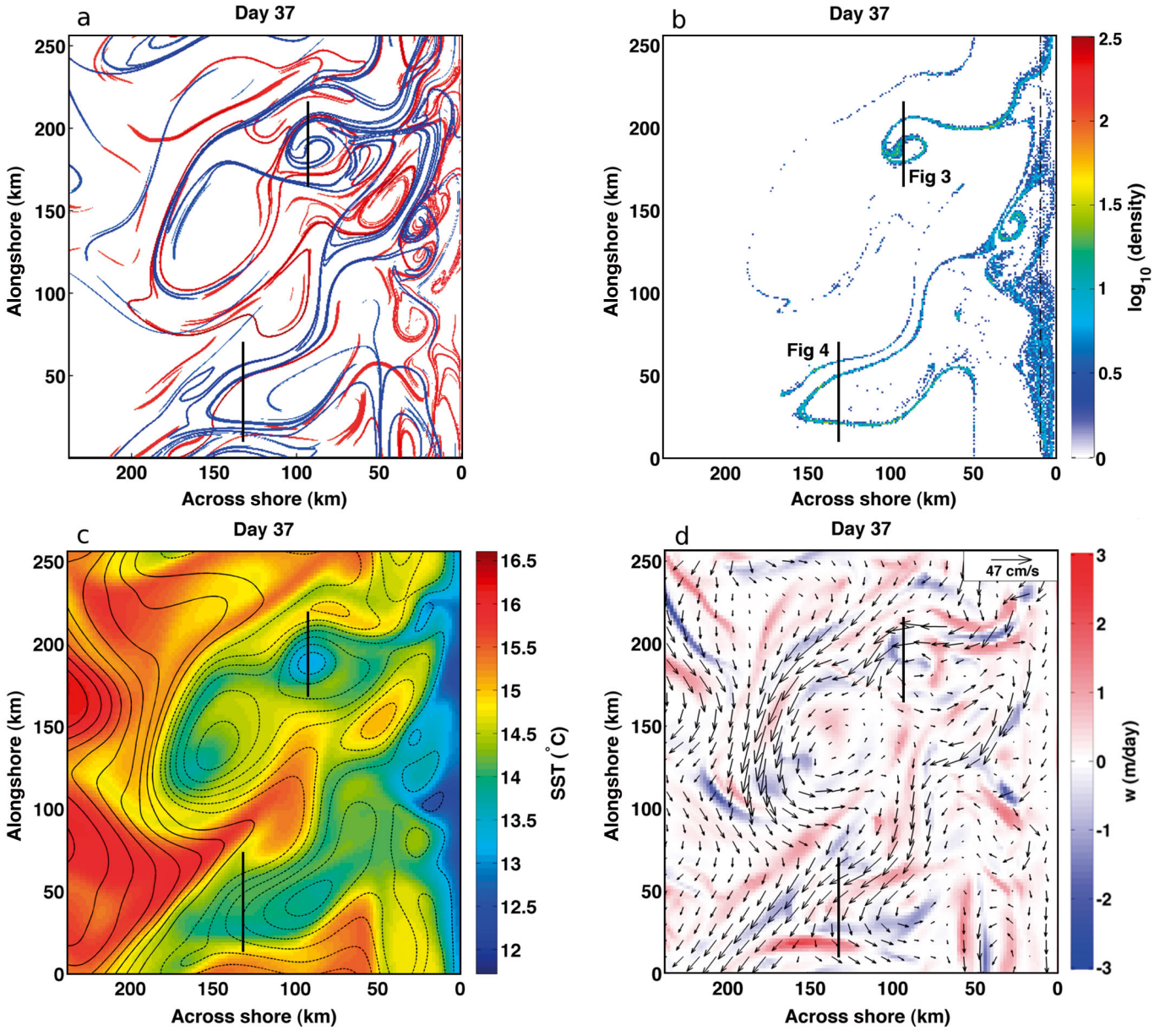

Fig. 2. Comparison of Eulerian and Lagrangian surface fields. (a) Lagrangian coherent structures (LCS). Blue and red lines represent attracting and repelling LCS, respectively. (b) Larval density (larvae km^{-2}), binned to 1 km squares and shown in a log scale as larvae are highly concentrated in narrow regions; simulated larvae were released inshore of the dashed line. (c) Sea-surface temperature (SST, color) with sea-surface height (SSH, contours); contour interval is 1 cm. (d) Surface horizontal velocity (arrows) and near-surface (color, second model level ~5 m depth, positive upwelling) vertical velocity for Day 37 in Model Run 111. Larvae are primarily located in filaments that correspond to attracting LCS, SST fronts, and enhanced vertical velocities on either side of the filament. Bold black lines represent the transects shown in Fig. 3 (north) and Fig. 4 (south)

propagule transport into a horizontal, 2-dimensional, time-dependent problem. Note we will use larva, particle, and propagule interchangeably with the understanding that we mean modeled, surface-following particles for each of these terms. For both the larval transport and LCS calculations, particle positions are integrated in time using a fourth-order Runge-Kutta scheme with the ROMS-simulated surface velocities (saved every 6 h) interpolated to the particle locations each integration time step. Larvae are released daily from Day 0 to Day 170 within the shelf zone (<10 km offshore) on a regular 2 km grid and tracked from the time of release until the end of each 180 d run; effectively we are assuming all shelf areas are larval source regions and that larvae are continuously released. Because larval mortality is not modeled, the

number of larvae (and the range of ages since release of those larvae) increases with time. Each tracer particle is considered to potentially represent a large number of actual larvae because individuals of many species release thousands to millions of larvae at one time (e.g. Love et al. 2002, Mitarai et al. 2008, 2009).

RESULTS

LCS, filamentation, and larval density patterns

Flow features produced in the model (Fig. 2) broadly resemble those observed, both off California (Flament et al. 1985, Brink & Cowles 1991) and in other eastern boundary currents (Haynes et al. 1993, Hill et al. 1998). Instabilities in the upwelling jet produce eddies and upwelling filaments, which are fast, relatively narrow (on the order of 10s of kilometers wide) features with coherent flow reaching 100s of meters deep into the water column that can quickly move material offshore (Flament et al. 1985). As these upwelling filaments and other flow features interact with the eddy field offshore, they are further stirred and filamented, resulting in a patchy distribution of larvae (Video S2 in the supplement at www.int-res.com/articles/suppl/m472p027_supp/).

Inspection of the larval density field demonstrates that the transport of coastal material predominantly occurs in long, thin, spatially connected filaments (Fig. 2b). Similarly patchy density distributions are seen throughout this model run (Video S2 in the supplement) as well as all other runs. Regions of high larval density are observed to correspond with ALCS, but only sometimes with RLCS (Fig. 2a,b). Coincidence of filaments, LCS, and surface variables is illustrated in Figs. 3 & 4, where transects are taken across 2 regions (bold vertical lines in Fig. 2). Fig. 3 transects a filament in 3 places as it spirals into a cyclonic eddy. Fig. 4 transects 2 filaments; 1 filament is crossed twice as it is swept shoreward around an elongated eddy. Transects of the forward and backward FTLE fields are plotted in Figs. 3c & 4c; ALCS are marked with light gray bars and plotted on other panels. Regions of high density are found on or near ALCS (Figs. 3a & 4a). Conversely, not all ALCS correspond to regions of high larval abundance, as they are not connected to

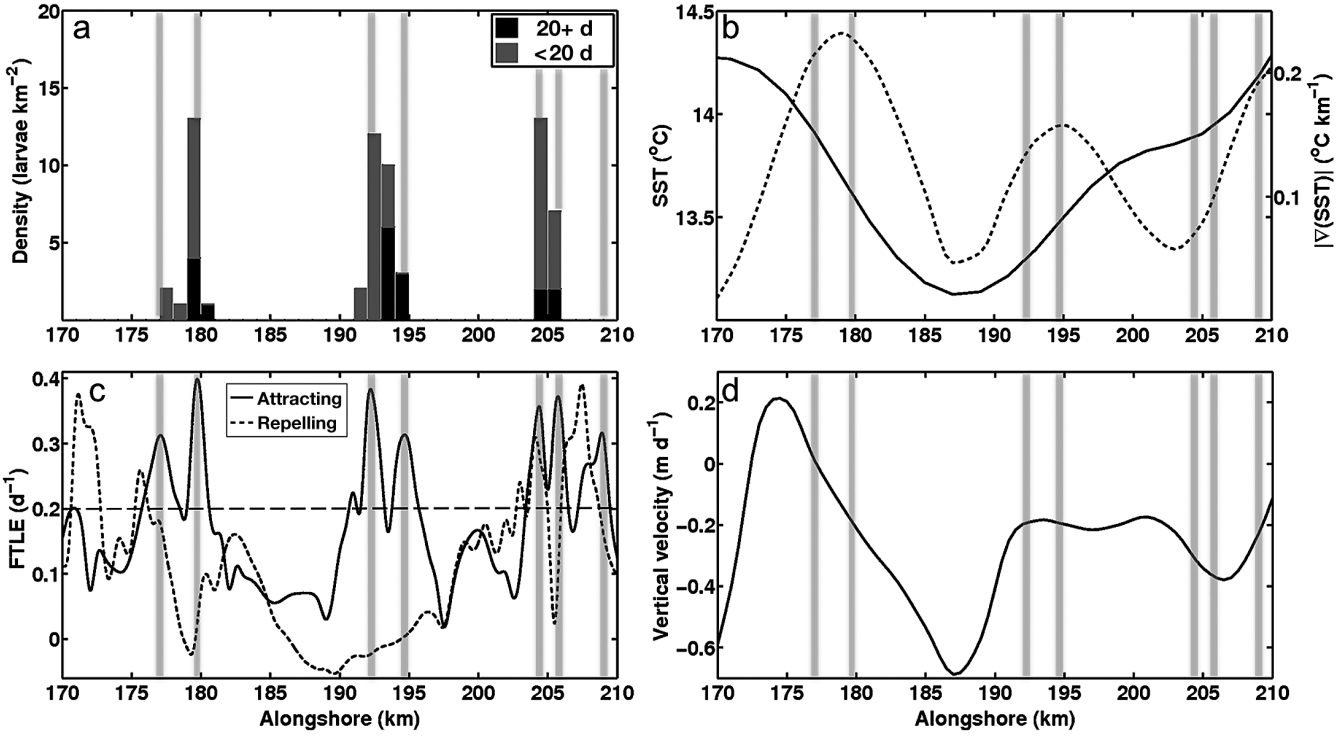

Fig. 3. North transect of model surface fields across a filament spiraling into an eddy (upper bold line in Fig. 2 panels). (a) Larval abundance is high in narrow regions corresponding to attracting Lagrangian coherent structures (ALCS, gray bars in a–d). (b) Sea-surface temperature (SST) gradient (dashed line) is high where LCS separate cold and warm water, SST shown in solid line. (c) LCS are found by identifying maxima of the finite-time Lyapunov exponent (FTLE). Horizontal dashed line corresponds to the statistical threshold for LCS. (d) Vertical velocities from the second model level (~5 m depth) are strongest on either side of the strongest temperature fronts (here at 180 km alongshore), with positive vertical velocity (upwelling) on the warmer side of the front as the ageostrophic circulation attempts to stratify the front

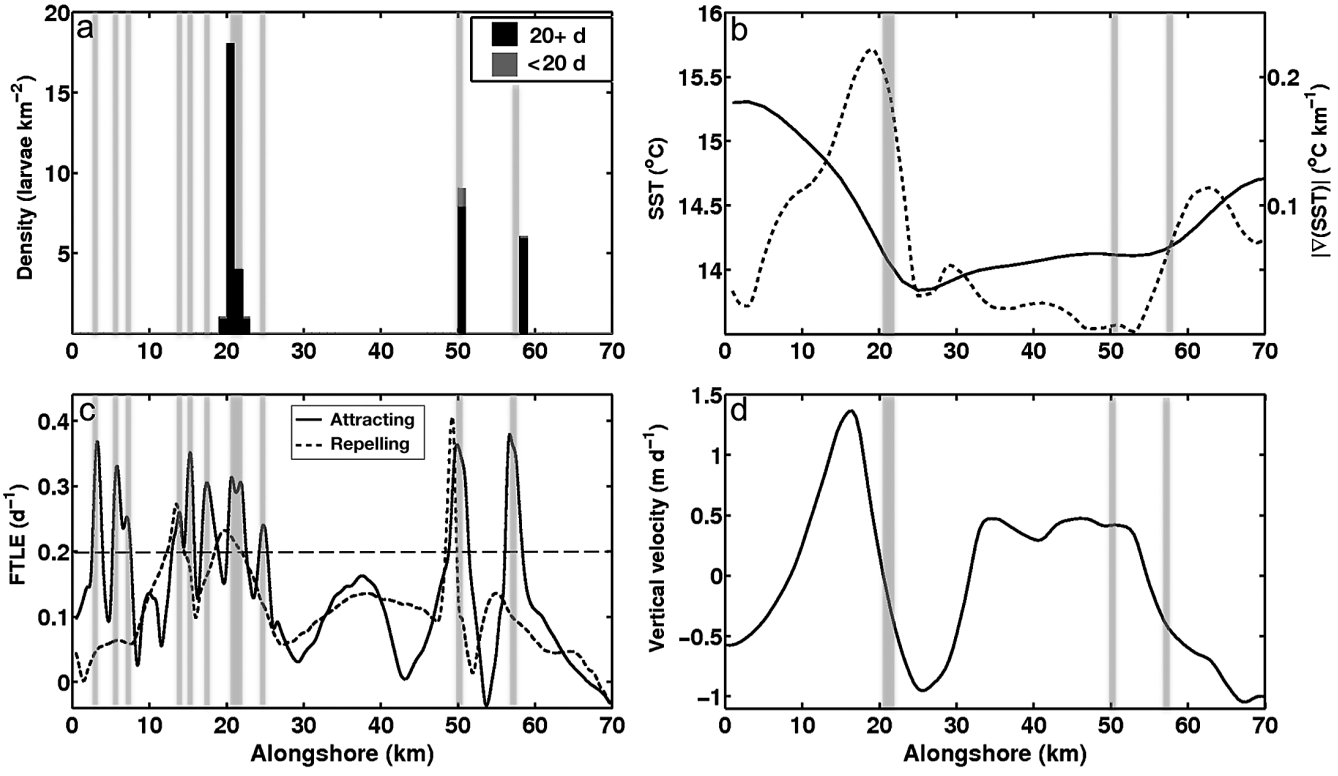

Fig. 4. South transect of model surface fields across 2 filaments (lower bold line in Fig. 2). Model fields are as in Fig. 3. Note that not every ALCS (gray bars) corresponds to a filament containing coastal material and that some regions of larval filamentation do not correspond with temperature fronts but are still marked by LCS (here at 50 km alongshore) in (a) and (b), respectively

a region where particles were released (cf. Fig. 4a,c). Regions of high larval concentration only sometimes coincide with RLCS, which are found using high values of the forward FTLE field (red in Fig. 2a, short-dashed lines in Figs. 3c & 4c); coincidence mainly occurs when the RLCS are also close to ALCS (e.g. Fig. 4c at 50 km).

To assess the relationship between LCS and filaments, statistics of the forward (FFTLE) and backward (BFTLE) FTLE fields throughout the model domain were compared to the values of these fields interpolated to particle positions. We asked the following: (1) How often are larvae on an LCS? and (2) Which type of LCS do they end up on? Complementary cumulative distribution functions for BFTLE and FFTLE values are shown in Fig. 5a for a single day (Day 37, also shown in Fig. 2) and in Fig. 5b for a 100 d ensemble. Cumulative distribution functions for the FTLE values are calculated for the entire domain (black lines in Fig. 5a,b) and for where particles are located (blue and red lines). Pairwise comparisons of cumulative distribution functions (BFTLE vs. BFTLE at particle positions, FFTLE vs. FFTLE at particle positions, and BFTLE at particle positions vs. FFTLE at particle positions) were done using a Kolmogorov-Smirnov test. All pairs of distributions were significantly different ($p < 0.001$), as expected given the large number of data points ($n > 10^4$ for all distributions).

Particles were determined to be on or sufficiently near an LCS when the FTLE values at their positions were >0.2 d^{-1} (shown in Figs. 3c & 4c as a horizontal dashed line). This threshold is determined experimentally and depends on ocean dynamics and the FTLE integration time. FTLE field statistics at the particle positions were compared to FTLE statistics for the entire domain. Larvae were more likely on an LCS (40 to 60%) than if they were randomly distributed (~25% of all larvae expected for Day 37; Fig. 5a). Furthermore, for Day 37, larvae were much more likely to be on ALCS (~60% of all larvae) than on RLCS (~40% of all larvae), as is consistent with the arguments presented in the section 'Lagrangian coherent structures'. Extending the analysis to a 100 d ensemble (Fig. 5b), larvae were more likely on LCS (25 to 40%) than if they were randomly distributed (~20%), and again more likely on ALCS (~40% of all larvae) than on RLCS (~25% of all larvae). This suggests filamentation mapped by LCS plays an important role in transport of material originating over the shelf in EBCs.

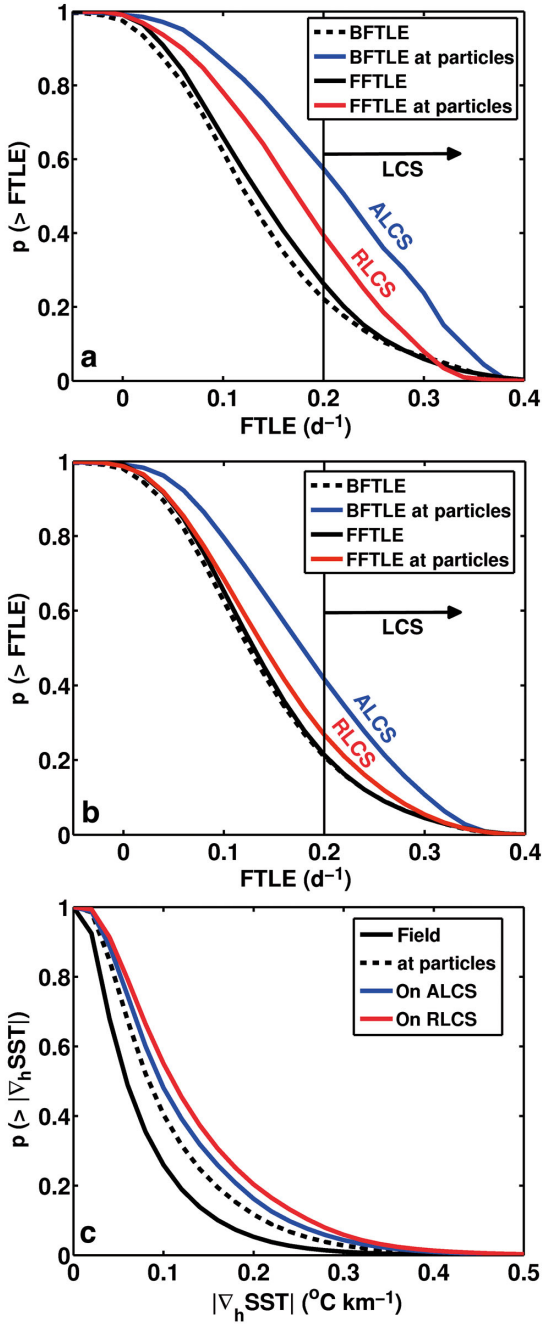

Fig. 5. Comparison of backward (BFTLE) and forward (FFTLE) finite-time Lyapunov exponent statistics for (a) the day shown in previous figures and (b) a 100 d ensemble. (c) Sea-surface temperature gradient statistics (∇_hSST, in °C km^{-1}) are also shown for the 100 d ensemble. Cumulative distribution functions have been summed from the highest to lowest values. Lagrangian coherent structures (LCS) are defined here by values of FTLE fields >0.2 d^{-1} (vertical lines). In general particles are more often on LCS than if they were randomly distributed (black lines), and especially more likely to be on attracting (blue, ALCS) than repelling (red, RLCS) LCS. Likewise particles are more likely to be on temperature fronts (high ∇_hSST) than if they were randomly distributed, and even more likely when they are on ALCS or RLCS

Filaments and fronts

In the CCS-in-a-box model, larval filaments marked by LCS are often found between cyclonic (cold-core) and anti-cyclonic (warm-core) eddies (Figs. 2 to 4). Hence, larval filaments are also associated with high sea-surface temperature (SST) gradients, consistent with larval surveys in the CCS (e.g. Larson et al. 1994). However, the transects in Fig. 4 show some cases where LCS and high particle densities are not coincident with a SST front (e.g. at 50 km alongshore in Fig. 4). To test the relationship of LCS and SST fronts we asked: If a particle is on an LCS, how much more likely is it to be on a front? Fig. 5c compares the complementary cumulative distribution of the horizontal (surface) SST gradient magnitude $|\nabla_h SST|$ with the distribution at all particle positions and for particles near LCS (FTLE > 0.2 d^{-1}) over the 100 d ensemble. Particles were more likely to be on higher values of $|\nabla_h SST|$ than if randomly distributed (e.g. 40% above 0.1°C km^{-1}, ~25% expected), while particles on or near LCS were even more likely to be on high $|\nabla_h SST|$ values (50 to 60% above 0.1 °C km^{-1}, twice as many as expected; $p < 0.001$ for all comparisons). This demonstrates that larvae are more likely to be on fronts, especially those also on a LCS.

Regions of high SST gradients are observed to be associated with locally enhanced vertical velocities on the second model layer (~5 m) on either side of the front (and thus LCS; Figs. 2d, 3d & 4d), consistent with a secondary ageostrophic circulation attempting to stratify the front (e.g. Capet et al. 2008, Klein & Lapeyre 2009). Frontal vertical velocities are difficult to correlate statistically with SST fronts (and by extension LCS and filaments) since they are maximal at either side of the front and not along it (Capet et al. 2008). Possible implications are discussed in 'Comparisons with observations and prior studies'.

Eddy–eddy interactions, source regions, and larval age distributions

The ages of larvae along filaments are generally older the farther out to sea they are from their initial release location, as has been observed *in situ* (Rodriguez et al. 1999). In Fig. 3 each of the 3 filament crossings are at a different oceanographic (or integrated path) distance from the shelf. Larvae are shown in 2 age classes: 0 to 20 d old and 20 d and older (Fig. 3a). Along the filament, a higher abundance of older larvae is found in regions that are further from shore. This age pattern is also seen in the southern

transect (Fig. 4a), where both filaments are farther in a path sense, from the source region than in the eddy transect. Here larvae are older, with the age gradient of larvae along the twice-crossed filament increasing with oceanographic distance from shore.

In contrast to these simple examples, the interaction of larval filaments and eddies can result in complex density and age-structure patterns. As an example of this process, a time series of eddy interaction, merging, and larval particle packet formation is shown in Fig. 6. Here, a 25 km diameter cyclonic eddy is formed initially near the shelf with a mass of simulated larvae spiraling into its center (Day 91, Eddy 1). This small eddy interacts with a similarly sized eddy (Eddy 2), and a larger cyclonic eddy (Eddy 3) over a 10 d period (Days 94 to 103), which can be visualized by the particle density field, the LCS locations, and the sea-surface height (SSH; Fig. 6). During the interaction, both particle density and LCS distributions show that the contents of Eddy 1 are compressed and filamented around the periphery of the larger eddy, resulting in a thin, dense packet of material that was formerly the core of Eddy 1 being transported back towards the coast along the larger eddy's exterior. In contrast, the SSH signatures of the 2 small eddies appear to merge during the interaction (Fig. 6; Day 97), illustrating that what is observed in the Eulerian frame (SSH) does not necessarily determine the transport fate of larval particles (the time-integrated Lagrangian flow), as has often been noted in the dynamical systems literature (i.e. Shadden et al. 2005). The packet has a maximal density of >90 particles km^{-2}, roughly 2 orders of magnitude greater than the initial particle release density (<1 larva km^{-2}). Note that many LCS are swept together and combined as the packet is formed, and the resulting large number of collinear ALCS are coincident with striations of dense material (Fig. 6; Day 103). This striated pattern of planktonic material is similar to patterns seen *in situ* in the CCS (Mackas et al. 1991).

Packets formed by eddy interactions are often comprised of a wide range of larval age classes from many source locations, concentrated in a very small spatial area. The dense packet shown in Fig. 6 (black line on Day 103) contains larvae ranging from <20 to >60 d old (Fig. 7a). The material in the densest portion of the packet (22 to 23 km alongshore in Fig. 7a), representing a 1 km^2 bin in Fig. 6, came from sources up to 50 km south and 220 km north of the packet location on Day 103 (Fig. 7b), where the source regions have been unwrapped to account for the periodic boundary in the ocean circulation model. Notably some of this material came from south of its current location, having traveled against the average southward alongshore flow.

Filamentation can lead to a quick trip offshore, decreasing transit time away from the shelf. For example, on Day 177 particles ranging from 7 to 29 d old are found >150 km offshore, concentrated in a filament that wraps around the periodic model boundary (Fig. 8a; denoted by Xs). Conversely filaments often bend back toward the coast or get folded into a persistent retention zone (i.e. an eddy), resulting in older larvae being transported back towards the shelf. Inshore of the example filament described above are many regions of older larvae (30 to 120+ d old; Fig. 8b–e); we will focus on 2 of these areas, marked in boxes in Fig. 8f. Histograms of source locations and age distributions for the 2 boxed regions are shown in Fig. 9.

For the coherent structure on Day 177 (dashed box in Fig. 8f), again a large number of larvae with a diverse range of ages have been concentrated into a small region (see Video S2 in the supplement). There are >15 000 particles in this structure, 16% of the total number of particles in the entire domain at this time. Within the coherent structure particles range from 40 to 170 d old and are from source regions spanning 150 to >800 km alongshore (Fig. 9a,b). Note that in Fig. 9a the tails of the distribution are not completely shown and some larvae originate from source locations >1200 km alongshore (having crossed the periodic domain 4 times). Some larvae older than 120 d are within 50 km of the coast (solid box in Fig. 8f). This packet contains particles ranging from 20 to 170 d old and from −10 to 500 km alongshore (Fig. 9c,d). Thus, eddy interaction may result in transport of material back to the shelf (and for some larvae back to their source locations) long after release.

Dense larval packets resulting from complex and variable eddy–eddy interaction and filamentation processes are found throughout this model run (see Videos S1 & S2 in the supplement) and in all other model runs. To assess the average statistics of packet formation and their associated larval age and source distributions, we evaluate a 'packet' over a 1 km^2 region. Fig. 10 shows the complementary cumulative distribution of packet densities at each larva position over the model run shown in other figures. In most cases larvae are in packets many times denser than their release densities (<1 km^{-2}; i.e. $p = 0.54$ for density >5 km^{-2}). Average age and source histograms were determined for very dense packets (density > 50 km^{-2}, $p = 0.06$, gray shading in Fig. 10; $n = 8140$ packets) by subtracting the mean values for each packet and combining (Fig. 10 inset; $n = 7 \times 10^5$ particles in total). Standard deviations are 73 km for

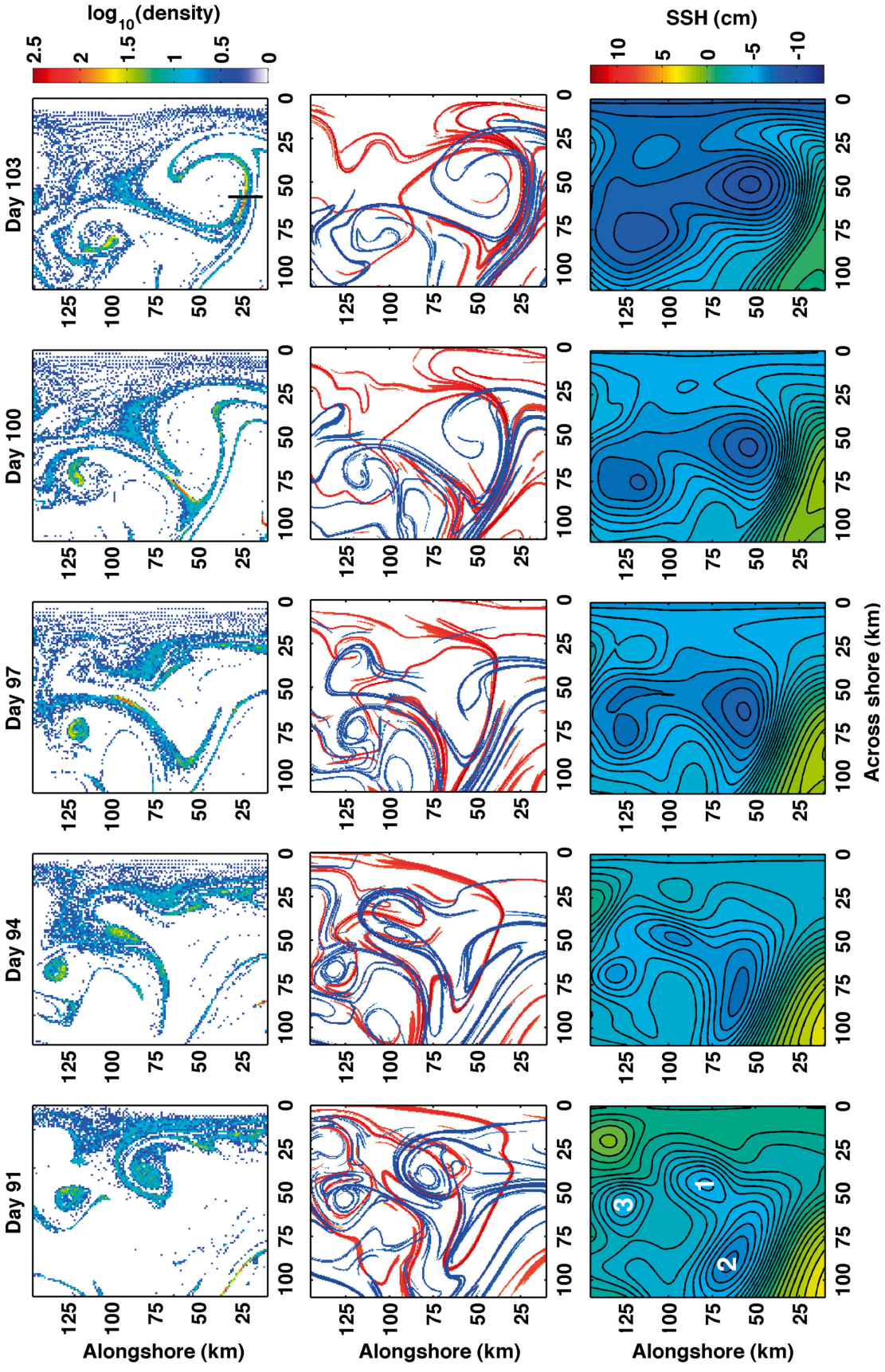

Fig. 6. Interaction of anticyclonic eddies over Model Days 91 to 103 leads to the formation of a dense accumulation of larvae in a narrow filamental packet. Top row: density of all age classes (particles km^{-2}, shown on a log scale). Middle row: attracting (blue) and repelling (red) Lagrangian coherent structures. Bottom row: sea-surface height (SSH) with 0.5 cm contour interval. Note this is a subregion of the model domain shown in other figures. Numbers in the lower left panel refer to eddies mentioned in the text. The black line in the upper right panel indicates the transect of larval density shown in Fig. 7

source regions and 14 d for ages in packets, with long tails for both histograms as seen in previous examples. These results suggest that, on average, dense regions of larvae will contain larvae from a wide range of source locations and release times. Since mesoscale eddy interaction processes are similar throughout the global ocean (McWilliams 1984, Bracco et al. 2004), dense packets of floating larvae and similar biological materials are expected across a range of marine ecosystems.

DISCUSSION

Application of LCS

LCS have the potential for being used operationally to track regions of dense planktonic accumulation. Given availability of high-quality ocean surface velocity fields (i.e. high-frequency radar, operational data-assimilative coastal ocean models), attracting LCS can be assessed for connection to spawning regions and tracked through time (Coullette et al. 2007, Shadden et al. 2009). LCS also provide a powerful conceptual tool for understanding the kinematic framework that larval transport dynamics rests in, as LCS make the connection between filamentation, transport boundaries, and frontal processes. Further, results from dynamical systems theory can be applied to predict the sensitivity of ecological processes associated with LCS.

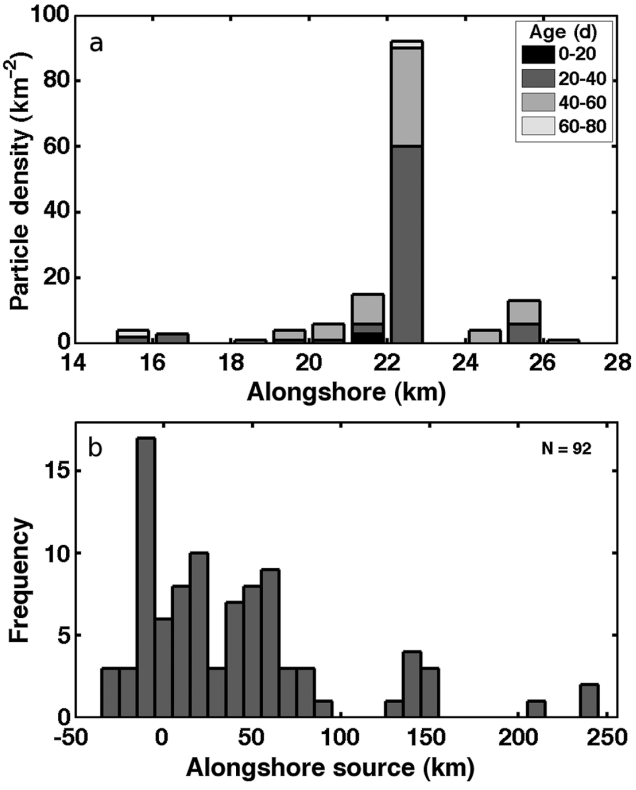

Fig. 7. (a) Transect of larval density from 56 km offshore on Model Day 103 (along the vertical black line in the upper right panel in Fig. 6), with age-class distinctions (in days, grayscale). Ages range from <20 to >60 d within a narrow spatial region. (b) Larvae in the densest part of the larval packet (22 to 23 km alongshore, 92 particles) come from a wide range of source locations, where source regions have been unwrapped to account for transport across the periodic boundary in the ocean circulation model. Bin size for this histogram is 10 km; the vertical axis is the number of particles from each source region

The importance of horizontal swimming provides an excellent example of how dynamical systems results can be applied to the larval transport problem. Clearly larval swimming is difficult to model, involving species-specific assumptions about cues, swimming duration, speed, and direction (e.g. Metaxas & Saunders 2009). Since LCS are structurally stable and therefore largely insensitive to perturbation (Haller 2002, Harrison & Glatzmaier 2012), it follows that up to a certain swimming speed in *any* direction, or for short, strong bursts of swimming, larvae will effectively remain on LCS. To provide a rough demonstration of this stability, Fig. 11 shows the effect of normally distributed, random-walk horizontal 'swimming' on the density patterns shown in Fig. 8f. The random-walk perturbations were added with standard deviations σ of 1 and 10 cm s^{-1}. For both cases the horizontal swimming direction and magnitude was randomized at each particle time step. For a perturbation of σ = 1 cm s^{-1}, density patterns are very similar to their original distributions (compare Figs. 8f & 11a). At a perturbation level of σ = 10 cm s^{-1} (much higher than the expected swimming speeds of most early stage larvae; e.g. Love et al. 2002, Metaxas & Saunders 2009), packets and filaments are still in evidence. Maximum concentrations have been reduced compared with the non-swimming case, but they are still an order of magnitude higher than the release density (Fig. 11b). Thus, we expect filaments and eddies are robust aggregators of planktonic and nektonic organisms even under a wide range of (slow) behavioral strategies.

Comparisons with observations and prior studies

The present analyses linking processes of filamentation and larval distributions should be widely applicable, as upwelling dynamics are similar across all EBCs (e.g. Haynes et al. 1993, Hill et al. 1998). For

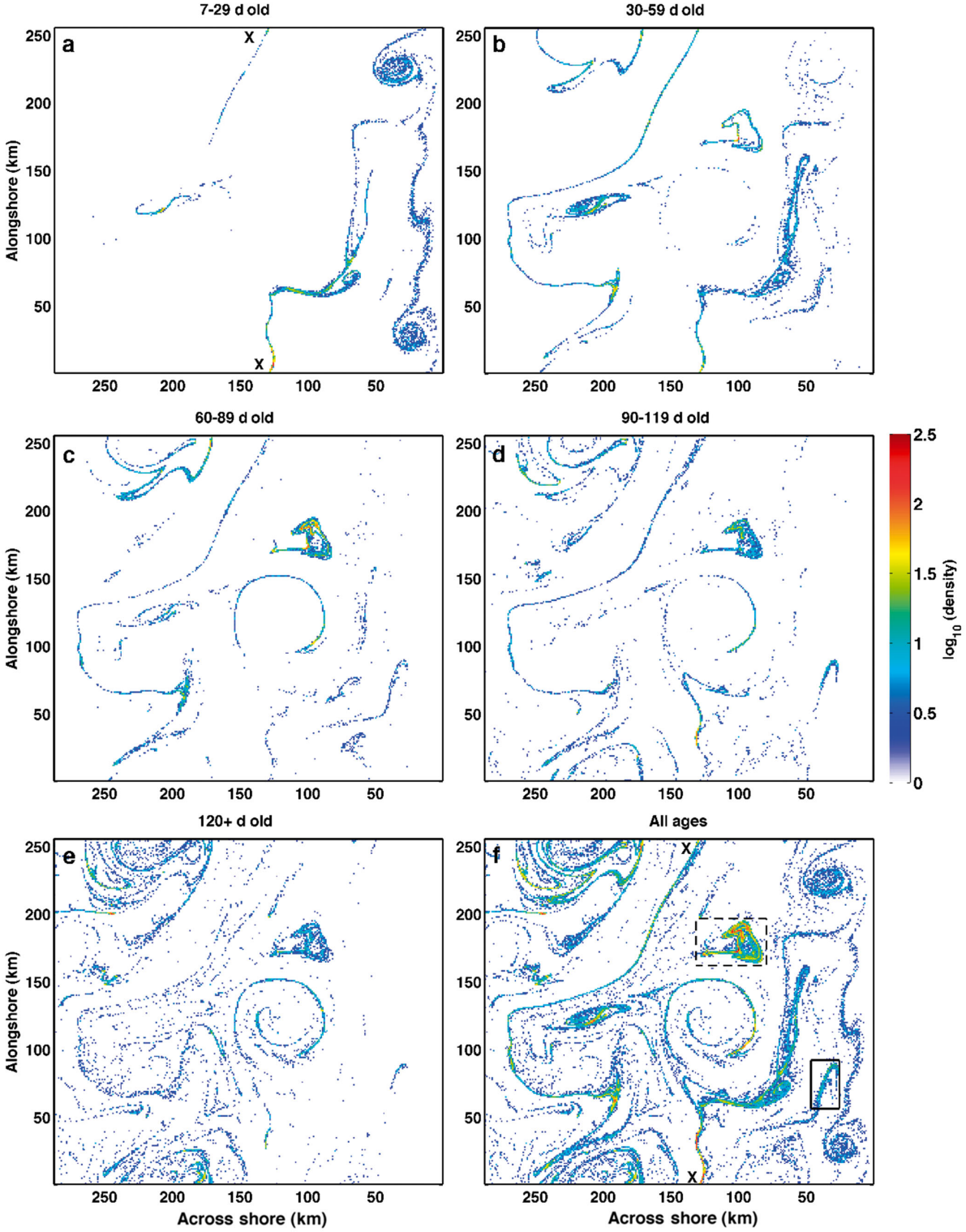

Fig. 8. Density distributions by age class on Model Day 177 are shown for ages (a) 7 to 29 d, (b) 30 to 59 d, (c) 60 to 89 d, (d) 90 to 119 d, (e) 120 d and over, and (f) all age classes. Larval density (particles km^{-2}) is shown on a log scale to facilitate visualization. Note the feature centered at 100 km offshore and 175 km alongshore (dashed box, f) has integrated particles from many different age classes (b–e), and that some particles are near the coast (<50 km) even after 120 d (solid box, f). In contrast, young larvae (a) have reached upwards of 150 km offshore in a fast-moving filament (denoted by '**X**') that wraps around the periodic model boundary. See Video S2 in the supplement for visualization of density through the model run. Age and source distributions for the boxed regions are shown in Fig. 9

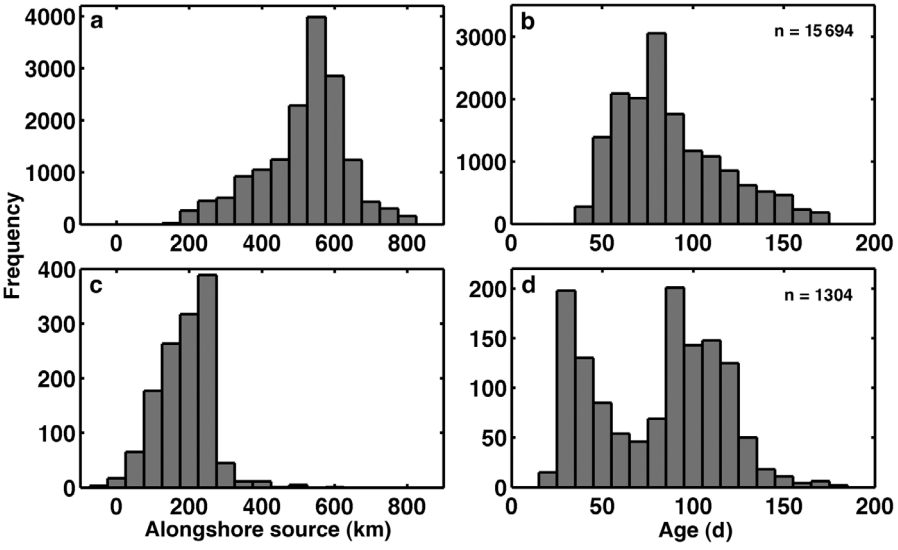

Fig. 9. Histograms of (a,c) source locations and (b,d) age distributions for the 2 boxed regions in Fig. 8f. In both cases larvae from a wide range of sources and release times are found in the same region. The coherent structure (dashed box, Fig. 8f) has integrated larvae originating from 150 to >800 km alongshore (a), and contains particles ranging from 40 to 170 d old (b). A coastal packet (solid box, Fig. 8f) has particles that came from −10 to 600 km alongshore (c), and are <30 to >175 d old (d). Source locations have been unwrapped as in Fig. 7, with a bin size of 50 km. Age bins are 10 d wide. n is the total number of particles in the histogram. Note the difference in vertical scales for each plot

example, neritic larvae and coastal planktonic species are persistently found in upwelling filaments and their associated eddies in the Canary EBC (Rodriguez et al. 1999, Bécognée et al. 2009), and this is thought to be an important larval transport pathway from the mainland to offshore islands. In the CCS, the transport of propagules in filaments is consistent with the observed higher abundance of larvae at fronts (Larson et al. 1994, Bjorkstedt et al. 2002), although to our knowledge these 2 phenomena have not previously been connected. Packet formation and transport by eddy–eddy interaction and filamentation processes may explain the delivery of discrete settlement pulses of larvae that contain a wide range of age classes and species, and also contribute to shorter than expected dispersal distances (Warner et al. 2000, Warner & Cowen 2002, Siegel et al. 2008, Shanks 2009). These observations may be explained to leading order by ocean transport and passive particles, without invoking complex larval behavior or life histories.

Larval concentration in filaments may explain regions of predictably higher settlement downstream from headlands (Ebert & Russell 1988), as well as preferential spawning areas observed at submerged promontories (Karnauskas et al. 2011). Instead of adding more variability, a complex coastline will often organize the flow into more regular and predictable patterns. When an alongshore current reaches a coastal headland it is directed offshore, often forming a filament or eddy (Haynes et al. 1993, Kim & Barth 2011), and so can regularly generate high larval concentrations, making these areas advantageous spawning grounds (Karnauskas et al. 2011). If this concentrated material were directed back to shore it would result in a large, perhaps quick settlement pulse over a narrow coastal area downstream from a promontory, as seen in modeling studies (Kim & Barth 2011). Such settlement pulses are expected to correlate with frontal arrival,

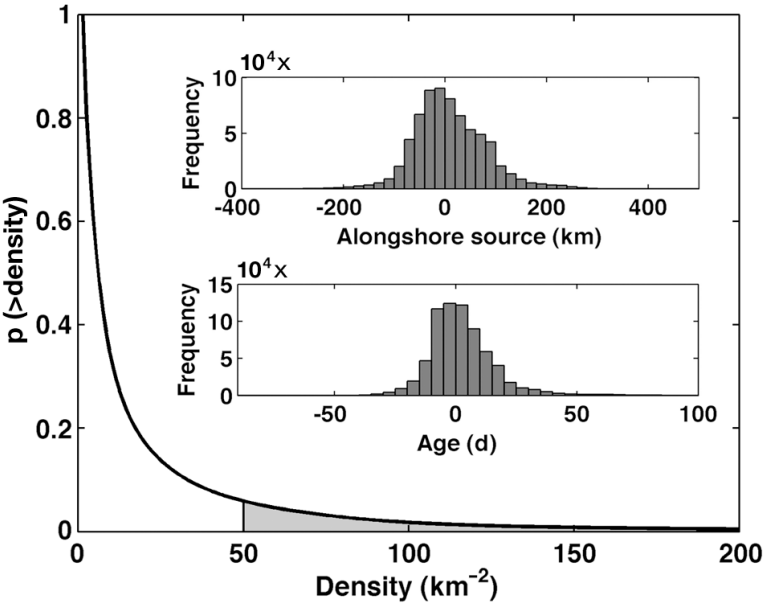

Fig. 10. Complementary cumulative distribution of density at particle locations shows that over the model run 6% (p = 0.059) of particles are found in packets (shaded gray, defined by density > 50 in a 1 km^2 bin). Combined histograms (with source and age averages removed for each packet) show a wide range of source regions (inset top) and ages (inset bottom) for larvae in packets. Horizontal axes on histograms show a portion of the long tails for each distribution

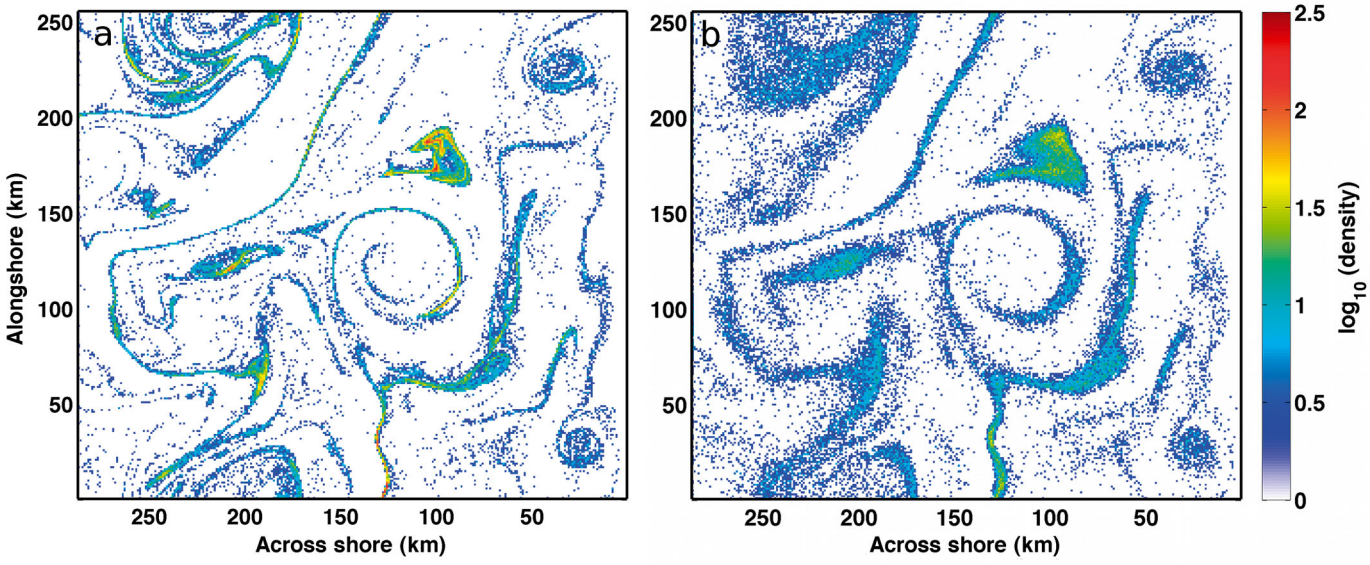

Fig. 11. Effect of swimming on density patterns. Density distributions are shown as in Fig. 8f with addition of random-walk type swimming at 2 levels: (a) 1 cm s^{-1} and (b) 10 cm s^{-1} standard deviation. As expected given the structural stability of Lagrangian coherent structures, dense packets and filaments are robust to a high degree of perturbation

as has been observed in the CCS (Bjorkstedt et al. 2002, Woodson et al. 2012).

Recent modeling studies suggest packet delivery back to the shore is a common phenomenon. Packet delivery will manifest in connectivity diagrams (Cowen et al. 2006, Siegel et al. 2008) as a linear feature, indicating a wide range of source regions were deposited at 1 arrival location (as in Fig. 7). This pattern is prominent in many EBC connectivity studies (Aiken et al. 2011, Drake et al. 2011, Kim & Barth 2011), notably for both non-buoyant and vertically migrating larvae, and is more prevalent for longer pelagic larval duration (PLD). However, it is unclear from these studies if linear connectivity patterns are due to single events or accrue over longer timescales. Since packet formation appears to be a consequence of the eddy–eddy interaction and filamentation processes, we expect it will occur across all ocean regions and likely generates the patterns seen in these studies.

Biophysical and trophic interactions along coastal upwelling filaments and fronts could influence larval survivability. Primary production is observed to be higher in upwelling filaments, as nutrient-rich water is carried offshore (Brink & Cowles 1991, Mackas et al. 1991, Hill et al. 1998), and also along fronts, where both planktonic and fish biomass can be enhanced (e.g. Landry et al. 2012). In addition, frontal vertical velocities due to submesoscale instabilities have been shown in coupled physical–ecosystem models to induce nutrient injection and increase productivity, but they also induce export materials from the euphotic zone (for reviews see Lévy 2008, Klein & Lapeyre 2009). Further, seabirds, fish, and other marine animals are known to use fronts for foraging and efficient transport (e.g. Fiedler & Bernard 1987, Tew Kai et al. 2009, Munk et al. 2010), indicating increased predation susceptibility for larvae at fronts. Larval survivability on a filament will be controlled by a combination of enhanced fitness due to food availability, higher mortality due to vertical export, or locally enhanced predation.

Many EBCs have wider shelves than the California coastline, such as those off Africa and the Iberian Peninsula. For these systems, upwelling can be centered at the shelf break, creating a kinematic boundary between a poleward shelf flow and the equatorward upwelling jet (Peliz et al. 2002). This on-shelf/shelf-break flow partitioning appears to depend on the details of both the pycnocline and wind forcing (Estrade et al. 2008), and has been observed to act as a retention mechanism for river outflow and very nearshore species (Santos et al. 2004). Similarly, observations (Hill et al. 1998) and more realistic models of the CCS often exhibit poleward flow close to the coast (e.g. Drake et al. 2011). We speculate that retention within this poleward flow, similar to the situation noted in studies off the Iberian Peninsula (Domingues et al. 2012), may limit the offshore extent of many intertidal and very nearshore spawners (Shanks & Shearman 2009), and perhaps contribute to the shorter than expected dispersal distances observed for some species (Shanks 2009). To our knowledge, it remains unclear what the temporal dynamics, response to wind variation, and 3-dimen-

sional kinematics are for this type of retention mechanism. However, the dynamical systems approach to identifying and classifying kinematic boundaries should be useful for diagnosing larval retention in these systems.

The breakdown of fronts by small eddies and meanders is readily seen in satellite observations (Flament et al. 1985); in ROMS these frontal instabilities are known to intensify with increasing model resolution (Capet et al. 2008). Such instabilities would likely lead to more mixing along filaments (Badin et al. 2011), but, to our knowledge, this has yet to be studied in the context of marine ecology. However, *in situ* measurements suggest that frontal accumulation of planktonic organisms in filaments is robust in the extension from model to reality (Larson et al. 1994, Rodriguez et al. 1999).

Potential roles of larval behavior

Many species' larvae and eggs are found preferentially near the ocean surface (e.g. Shanks 1985, Rodriguez et al. 1999, Bjorkstedt et al. 2002, Love et al. 2002, Metaxas & Saunders 2009). We have shown previously that random horizontal swimming will influence larval density patterns only for large swimming speeds (Fig. 11). In evaluating the effects of vertical swimming behavior, the particle model formulation used here assumes propagules swim or float to overcome the modest model vertical velocities (<5 m d^{-1}; Figs. 2 to 4), i.e. prefer to be in the productive euphotic zone. If particles were free to move vertically, this could result in a lesser degree of density enhancement; instead of aggregating at the surface, non-buoyant particles would be pushed down by surface convergence and downwelling (e.g. Bakun 2010). Though modeled vertical velocities here are instantaneously small, the accumulated effect over time can be large and will increase density patchiness (Zhong et al. 2012). Our analysis of transport boundaries and particle filimentation also applies to any floating material originating over the shelf (e.g. pollutants, macrophytes), and aggregations of these materials can form pelagic habitats for a variety of marine organisms (Shanks 1985, Dempster & Taquet 2004), indicating a possible secondary effect on larval distributions.

Previous results with the CCS-in-a-box model show ontogenetic vertical migration does not have strong effects on larval settlement statistics (Mitarai et al. 2008, Siegel et al. 2008). Upwelling filaments are generally coherent up to 100s of meters in depth (e.g. Brink & Cowles 1991), so it follows that with even a moderate change in vertical position larvae will remain within these flow structures. In contrast, regions with generally high vertical velocity shear, for example estuaries (North et al. 2008) or systems with bifurcations in major currents, such as off the north coast of Norway (Fiksen et al. 2007) or among coral reef habitats (Cowen & Sponaugle 2009), will be more sensitive to larval behavior. A common feature of EBCs is vertical shear between the coastal equatorward upwelling jet and the poleward undercurrent (Hill et al. 1998), and larval transport in this region is affected by diurnal vertical migration (Aiken & Navarete 2011). It still remains largely unclear where, when, and to what extent vertical swimming will be important given realistic flow fields.

SUMMARY

Larvae released above the shelf in an idealized EBC are often transported in filaments that coincide with LCS. Larvae are more likely to be found on an ALCS (~40% over a 100 d ensemble) than on a RLCS (~25%), and more likely on LCS than if they were randomly distributed (~20% expected). Larvae on LCS are also more likely to be on SST fronts (twice as many as expected for $|\nabla_h SST| > 0.1$°C km^{-1}), although this is not always the case. Eddy–eddy interaction and filamentation processes result in the creation of dense packets, which bring larvae of many age classes and source regions together into a small spatial region. Results are consistent with observations of larval distributions and settlement patterns in EBCs and other systems. Packet formation as a manifestation of eddy interaction and filamentation processes should occur globally. These packets sometimes get transported back to the coast, and the associated pattern of connectivity is seen in other studies. LCS are insensitive to a moderate degree of perturbation (e.g. swimming) and so are expected to be robust in mapping transport pathways under a variety of larval behavioral strategies.

Acknowledgements. Input from G. Glatzmaier and P. Raimondi was helpful in focusing this project, as well as overall support and writing assistance from R. Warner, K. Brink, A. Payton, and E. Silver. Four anonymous reviewers supplied thoughtful critiques that greatly improved the manuscript. This project was supported in part by NSF Grants OCE-030844 and OCE-1155813, by the Center for Stock Assessment Research (CSTAR), a partnership between NOAA Fisheries Santa Cruz Laboratory and UCSC, and by IGPP Santa Cruz.

LITERATURE CITED

Abraham RH, Shaw CD (1992) Dynamics—the geometry of behavior. Part 3: global behavior. Addison-Wesley, München

Aiken CM, Navarrete SA (2011) Environmental fluctuations and asymmetrical dispersal: generalized stability theory for studying metapopulation persistence and marine protected areas. Mar Ecol Prog Ser 428:77–88

Aiken CM, Navarrete CM, Castillo M, Castilla JC (2007) Along-shore larval dispersal kernels in a numerical ocean model of the central Chilean coast. Mar Ecol Prog Ser 339:13–24

Aiken CA, Navarrete SA, Pelegrí JL (2011) Potential changes in larval dispersal and alongshore connectivity on the central Chilean coast due to an altered wind climate. J Geophys Res 116(G4):G04026, doi:10.1029/2011JG001731

Badin G, Tandon A, Mahadevan A (2011) Lateral mixing in the pycnocline by baroclinic mixed layer eddies. J Phys Oceanogr 41:2080–2101

Bakun A (2010) Linking climate to population variability in marine ecosystems characterized by non-simple dynamics: conceptual templates and schematic constructs. J Mar Syst 79:361–373

Bécognée P, Moyano M, Almeida C, Rodríguez J, Fraile-Nuez E, Hernández-Guerra A, Hernández-León S (2009) Mesoscale distribution of clupeoid larvae in an upwelling filament trapped by a quasi-permanent cyclonic eddy off Northwest Africa. Deep-Sea Res I 56:330–343

Berkley HA, Kendall BE, Mitarai S, Siegel DA (2010) Turbulent dispersal promotes species coexistence. Ecol Lett 13:360–371

Beron-Vera FJ, Olascoaga MJ, Goni GJ (2008) Oceanic mesoscale eddies as revealed by Lagrangian coherent structures. Geophys Res Lett 35:7, doi:10.1029/2008GL033957

Bjorkstedt EP, Rosenfeld LK, Grantham BA, Shkedy Y, Roughgarden J (2002) Distributions of larval rockfishes *Sebastes* spp. across nearshore fronts in a coastal upwelling region. Mar Ecol Prog Ser 242:215–228

Bode M, Bode L, Armsworth PR (2011) Different dispersal abilities allow reef fish to coexist. Proc Natl Acad Sci USA 108:16317–16321

Botsford LW, Brumbaugh DR, Grimes C, Kellner JB and others (2009) Connectivity, sustainability, and yield: bridging the gap between conventional fisheries management and marine protected areas. Rev Fish Biol Fish 19:69–95

Bracco A, von Hardenberg J, Provenzale A, Weiss JB, McWilliams JC (2004) Dispersion and mixing in quasi-geostrophic turbulence. Phys Rev Lett 92:084501

Brink KH, Cowles TJ (1991) The coastal transition zone program. J Geophys Res 96(C8):14637–14647, doi:10.1029/91JC01206

Broitman BR, Blanchette CA, Menge BA, Lubchenco J and others (2008) Spatial and temporal patterns of invertebrate recruitment along the west coast of the United States. Ecol Monogr 78:403–421

Calil PHR, Richards KJ (2010) Transient upwelling hot spots in the oligotrophic North Pacific. J Geophys Res 115(C2):C02003, doi:10.1029/2009JC005360

Capet X, McWilliams JC, Molemaker MJ, Shchepetkin AF (2008) Mesoscale to submesoscale transition in the California Current system. Part II: frontal processes. J Phys Oceanogr 38:44–64

Chassot E, Bonhommeau S, Dulvy NK, Mélin F, Watson R, Gascuel D, Le Pape O (2010) Global marine primary production constrains fisheries catches. Ecol Lett 13:495–505

Chelton DB, Schlax MG, Samelson RM, de Szoeke RA (2007) Global observations of large oceanic eddies. Geophys Res Lett 34:L15606, doi:10.1029/2007GL030812

Costello C, Rassweiler A, Siegel DA, De Leo G, Micheli F, Rosenberg A (2010) The value of spatial information in MPA network design. Proc Natl Acad Sci USA 107:18294–18299

Coulliette C, Lekien F, Paduan J, Haller G, Marsden J (2007) Optimal pollution mitigation in Monterey Bay based on coastal radar data and nonlinear dynamics. Environ Sci Technol 41:6562–6572

Cowen RK, Sponaugle S (2009) Larval dispersal and marine population connectivity. Ann Rev Mar Sci 1:443–466

Cowen RK, Paris CB, Srinivasan A (2006) Scaling of connectivity in marine populations. Science 311:522–527

Dempster T, Taquet M (2004) Fish aggregation device (FAD) research: gaps in current knowledge and future directions for ecological studies. Rev Fish Biol Fish 14:21–42

Domingues CP, Nolasco R, Dubert J, Queiroga H (2012) Model-derived dispersal pathways from multiple source populations explain variability of invertebrate larval supply. PLoS ONE 7(4):e35794

d'Ovidio F, Fernández V, Hernández-García E, López C (2004) Mixing structures in the Mediterranean Sea from finite-size Lyapunov exponents. Geophys Res Lett 31:L17203, doi:10.1029/2009GL020328

d'Ovidio F, De Monte S, Alvain S, Dandonneau Y, Lévy M (2010) Fluid dynamical niches of phytoplankton types. Proc Natl Acad Sci USA 107:18366

Drake PT, Edwards CA, Barth JA (2011) Dispersion and connectivity estimates along the U.S. west coast from a realistic numerical model. J Mar Res 69:1–37

Ebert TA, Russell MP (1988) Latitudinal variation in size structure of the west coast purple sea urchin: a correlation with headlands. Limnol Oceanogr 33:286–294

Estrade P, Marchesiello P, Verdiere D, Colin A, Roy C (2008) Cross-shelf structure of coastal upwelling: a two dimensional extension of Ekman's theory and a mechanism for inner shelf upwelling shut down. J Mar Res 66:589–616

Fiedler PC, Bernard HJ (1987) Tuna aggregation and feeding near fronts observed in satellite imagery. Cont Shelf Res 7:871–881

Fiksen Ø, Jørgensen C, Kristiansen T, Vikebø F, Huse G (2007) Linking behavioural ecology and oceanography: larval behaviour determines growth, mortality and dispersal. Mar Ecol Prog Ser 347:195–205

Flament P, Armi L, Washburn L (1985) The evolving structure of an upwelling filament. J Geophys Res 90:11765–11778, doi:10.1029/JC090iC06p11765

Gaylord B, Gaines SD (2000) Temperature or transport? Range limits in marine species mediated solely by flow. Am Nat 155:769

Genin A, Jaffe J, Reef R, Richter C, Franks P (2005) Swimming against the flow: a mechanism of zooplankton aggregation. Science 308:860

Haller G (2002) Lagrangian coherent structures from approximate velocity data. Phys Fluids 14:1851–1861

Harrison CS, Glatzmaier GA (2012) Lagrangian coherent structures in the California Current System—sensitivities and limitations. Geophys Astrophys Fluid Dyn 106:22–44

Haynes R, Barton E, Pilling I (1993) Development, persistence, and variability of upwelling filaments off the

Atlantic Coast of the Iberian Peninsula. J Geophys Res 98(C12):22681–22692, doi:10.1029/93JC02016

Hill AE, Hickey BM, Shillington FA, Strub PT, Brink KH, Barton ED, Thomas AC (1998) Eastern ocean boundaries coastal segment. In: Robinson AR, Brink, KH (eds) The sea, Vol 11. John Wiley & Sons, London, p 29–67

Huhn F, von Kameke A, Pérez-Muñuzuri V, Olascoaga MJ, Beron-Vera FJ (2012) The impact of advective transport by the South Indian Ocean Countercurrent on the Madagascar plankton bloom. Geophys Res Lett 39:L06602, doi: 10.1029/2012GL051246

Jackson GA, Strathmann RR (1981) Larval mortality from offshore mixing as a link between precompetent and competent periods of development. Am Nat 118:16–26

Karnauskas M, Chérubin LM, Paris CB (2011) Adaptive significance of the formation of multi-species fish spawning aggregations near submerged capes. PLoS ONE 6:e22067

Katija K, Beaulieu WT, Regula C, Colin SP, Costello JH, Dabiri JO (2011) Quantification of flows generated by the hydromedusa *Aequorea victoria*: a Lagrangian coherent structure analysis. Mar Ecol Prog Ser 435:111–123

Kim S, Barth JA (2011) Connectivity and larval dispersal along the Oregon coast estimated by numerical simulations. J Geophys Res 116(C6):C06002, doi:10.1029/2010JC006741

Kinlan B, Gaines S (2003) Propagule dispersal in marine and terrestrial environments: a community perspective. Ecology 84:2007–2020

Klein P, Lapeyre G (2009) The oceanic vertical pump induced by mesoscale and submesoscale turbulence. Ann Rev Mar Sci 1:351–375

Landry MR, Ohman MD, Goericke R, Stukel MR, Barbeau KA, Bundy R, Kahru M (2012) Pelagic community responses to a deep-water front in the California Current Ecosystem: overview of the A-Front study. J Plankton Res 34(9):739–748

Largier JL (2003) Considerations in estimating larval dispersal distances from oceanographic data. Ecol Appl 13: 71–89

Larson RJ, Lenarz WH, Ralston S (1994) The distribution of pelagic juvenile rockfish of the genus *Sebastes* in the upwelling region off central California. Calif Coop Ocean Fish Invest Rep 35:175–221

Lehahn Y, d'Ovidio F, Lévy M, Heifetz E (2007) Stirring of the northeast Atlantic spring bloom: a Lagrangian analysis based on multisatellite data. J Geophys Res 112(C8): C08005, doi:10.1029/2006JC003927

Lehahn Y, d'Ovidio F, Lévy M, Amitai Y, Heifetz E (2011) Long range transport of a quasi isolated chlorophyll patch by an Agulhas ring. Geophys Res Lett 38:L16610, doi:10.1029/2011GL048588

Levin LA (2006) Recent progress in understanding larval dispersal: new directions and digressions. Integr Comp Biol 46:282

Lévy M (2008) The modulation of biological production by oceanic mesoscale turbulence. In: Weiss JB, Provenzale A (eds) Transport and mixing in geophysical flows. Springer, Heidelberg, p 219–261

Love M, Yoklavich M, Thorsteinson L (2002) The rockfishes of the northeast Pacific. University of California Press, Berkeley

Mackas D, Washburn L, Smith S (1991) Zooplankton community pattern associated with a California Current cold filament. J Geophys Res 96(C8):14781–14797, doi:10.1029/91JC01037

Mancho A, Small D, Wiggins S (2006) A tutorial on dynamical systems concepts applied to Lagrangian transport in oceanic flows defined as finite time data sets: theoretical and computational issues. Phys Rep 437:55–124

Marchesiello P, Estrade P (2009) Eddy activity and mixing in upwelling systems: a comparative study of Northwest Africa and California regions. Int J Earth Sci 98:299–308

Marchesiello P, McWilliams JC, Shchepetkin AF (2003) Equilibrium structure and dynamics of the California Current System. J Phys Oceanogr 33:753–783

Mathur M, Haller G, Peacock T, Ruppert-Felsot J, Swinney H (2007) Uncovering the Lagrangian skeleton of turbulence. Phys Rev Lett 98:144502

McWilliams JC (1984) Emergence of isolated coherent vortices in turbulent flow. J Fluid Mech 146:21–43

Metaxas A, Saunders M (2009) Quantifying the 'bio-' components in biophysical models of larval transport in marine benthic invertebrates: advances and pitfalls. Biol Bull 216(3):257–272

Mitarai S, Siegel DA, Winters KB (2008) A numerical study of stochastic larval settlement in the California Current system. J Mar Syst 69:295–309

Mitarai S, Siegel DA, Watson JR, Dong C, McWilliams JC (2009) Quantifying connectivity in the coastal ocean with application to the Southern California Bight. J Geophys Res 114 (C10):C10026, doi:10.1029/2008JC005166

Munk P, Hansen MM, Maes GE, Nielsen TG and others (2010) Oceanic fronts in the Sargasso Sea control the early life and drift of Atlantic eels. Proc R Soc Lond B 227: 3593–3599

North EW, Schlag Z, Hood RR, Li M, Zhong L, Gross T, Kennedy VS (2008) Vertical swimming behavior influences the dispersal of simulated oyster larvae in a coupled particle-tracking and hydrodynamic model of Chesapeake Bay. Mar Ecol Prog Ser 359:99–115

Okubo A (1980) Diffusion and ecological problems: mathematical models. Springer-Verlag, Berlin

Olascoaga MJ, Beron-Vera FJ, Brand LE, Koçak H (2008) Tracing the early development of harmful algal blooms on the West Florida Shelf with the aid of Lagrangian coherent structures. J Geophys Res 113:c12014, doi: 10.1029/2007JC009533

Palumbi S (2003) Population genetics, demographic connectivity, and the design of marine reserves. Ecol Appl 13: 146–158

Parrish RH, Nelson CS, Bakun A (1981) Transport mechanisms and reproductive success of fishes in the California Current. Biol Oceanogr 1:175–203

Peliz Á, Rosa T, Santos A, Pissarra J (2002) Fronts, jets, and counter-flows in the western Iberian upwelling system. J Mar Syst 35:61–77

Rassweiler A, Costello C, Siegel DA (2012) Marine protected areas and the value of spatially optimized fishery management. Proc Natl Acad Sci USA 109:11884–11889

Roberts CM (1997) Connectivity and management of Caribbean coral reefs. Science 278:1454–1457

Rodriguez JM, Hernández-León S, Barton ED (1999) Mesoscale distribution of fish larvae in relation to an upwelling filament off Northwest Africa. Deep-Sea Res I 46:1969–1984

Rossi V, López C, Hernández-García E, Sudre J, Garçon V, Morel Y (2009) Surface mixing and biological activity in the four Eastern Boundary Upwelling Systems. Nonlin Processes Geophys 16:557–568

Ryther JH (1969) Photosynthesis and fish production in the

sea. Science 166:72
Samelson RM (2013) Lagrangian motion, coherent structures, and lines of persistent material strain. Ann Rev Mar Sci 5(1) in press
Samelson RM, Wiggins S (2006) Lagrangian transport in geophysical jets and waves: the dynamical systems approach. Springer, New York, NY
Santos AMP, Peliz A, Dubert J, Oliveira PB, Angélico M, Ré P (2004) Impact of a winter upwelling event on the distribution and transport of sardine (*Sardina pilchardus*) eggs and larvae off western Iberia: a retention mechanism. Cont Shelf Res 24:149–165
Shadden SC (2005) LCS tutorial. Available at: http://mmae.iit.edu/shadden/LCS-tutorial/ (accessed 22 March 2012)
Shadden SC (2012) Lagrangian coherent structures. In: Grigoriev R, Schuster HG (eds) Transport and mixing in laminar flows: from microfluidics to oceanic currents. Wiley, New York, NY
Shadden SC, Lekien F, Marsden JE (2005) Definition and properties of Lagrangian coherent structures from finite-time Lyapunov exponents in two-dimensional aperiodic flows. Phys D 212:271–304
Shadden SC, Lekien F, Paduan JD, Chavez FP, Marsden JE (2009) The correlation between surface drifters and coherent structures based on high-frequency radar data in Monterey Bay. Deep-Sea Res II 56:161–172
Shanks AL (1985) Behavioral basis of internal-wave-induced shoreward transport of megalopae of the crab *Pachygrapsus crassipes*. Mar Ecol Prog Ser 24:289–295
Shanks AL (2009) Pelagic larval duration and dispersal distance revisited. Biol Bull 216:373–385
Shanks AL, Shearman RK (2009) Paradigm lost? Cross-shelf distributions of intertidal invertebrate larvae are unaffected by upwelling or downwelling. Mar Ecol Prog Ser 385:189–204
Shchepetkin AF, McWilliams JC (2005) The regional oceanic modeling system (ROMS): a split-explicit, free-surface, topography-following-coordinate oceanic model. Ocean Model 9:347–404
Siegel DA, Kinlan BP, Gaylord B, Gaines SD (2003) Lagrangian descriptions of marine larval dispersion. Mar Ecol Prog Ser 260:83–96
Siegel DA, Mitarai S, Costello CJ, Gaines SD, Kendall BE, Warner RR, Winters KB (2008) The stochastic nature of larval connectivity among nearshore marine populations. Proc Natl Acad Sci USA 105:8974
Sponaugle S, Cowen R, Shanks A, Morgan W and others (2002) Predicting self-recruitment in marine populations: biophysical correlates and mechanisms. Bull Mar Sci 70: 341–375
Strathmann R (1985) Feeding and nonfeeding larval development and life-history evolution in marine invertebrates. Ann Rev Ecol Syst 16:339–361
Tew Kai E, Rossi V, Sudre J, Weimerskirch H and others (2009) Top marine predators track Lagrangian coherent structures. Proc Natl Acad Sci USA 106:8245–8250
Warner R, Cowen R (2002) Local retention of production in marine populations: evidence, mechanisms, and consequences. Bull Mar Sci 70:245–249
Warner R, Swearer S, Caselle J (2000) Larval accumulation and retention: implications for the design of marine reserves and essential habitat. Bull Mar Sci 66:821–830
Watson J, Mitarai S, Siegel DA, Caselle JE, Dong C, McWilliams JC (2010) Realized and potential larval connectivity in the Southern California Bight. Mar Ecol Prog Ser 401:31–48
Watson JR, Hayes CG, Raimondi PT, Mitarai S and others (2011a) Currents connecting communities: nearshore community similarity and ocean circulation. Ecology 92: 1193–1200
Watson JR, Siegel DA, Kendall BE, Mitarai S, Rassweiler A, Gaines SD (2011b) Identifying critical regions in small-world marine metapopulations. Proc Natl Acad Sci USA 108:E907–E913
Watson JR, Kendall BE, Siegel DA, Mitarai S (2012) Changing seascapes, stochastic connectivity and marine metapopulation dynamics. Am Nat 180:99–112
Wiggins S (2005) The dynamical systems approach to Lagrangian transport in oceanic flows. Annu Rev Fluid Mech 37:295–328
Woodson CB, McManus MA, Tyburczy JA, Barth J and others (2012) Coastal fronts set recruitment and connectivity patterns across multiple taxa. Limnol Oceanogr 57:582–596
Zhong Y, Bracco A, Villareal TA (2012) Pattern formation at the ocean surface: *Sargassum* distribution and the role of the eddy field. Limnol Oceanogr: Fluid Environ 2:12–27

Editorial responsibility: Hans Heinrich Janssen, Oldendorf/Luhe, Germany

Submitted: October 7, 2011; Accepted: September 19, 2012
Proofs received from author(s): December 12, 2012